

## Improving ductility in ultrafine grained nickel with porosity and segregation via deformation

Y.H. Zhao<sup>a,\*</sup>, Q. Zhan<sup>b,c</sup>, T.D. Topping<sup>a</sup>, Y. Li<sup>a</sup>, W. Liu<sup>a</sup>, E.J. Lavernia<sup>a</sup>

<sup>a</sup> Department of Chemical Engineering and Materials Science, University of California, Davis, CA 95616, USA

<sup>b</sup> Department of Materials Physics and Chemistry, University of Science and Technology Beijing, Beijing 100083, People's Republic of China

<sup>c</sup> National Center for Electron Microscopy, Lawrence Berkeley National Laboratory, Berkeley, CA 94720, USA

### ARTICLE INFO

#### Article history:

Received 23 June 2009

Received in revised form 29 October 2009

Accepted 30 October 2009

#### Keywords:

Nanostructured Ni

Nano-porosity

Grain boundary segregation

Ductility

Deformation

### ABSTRACT

When bulk nanostructured (NS) materials are prepared via consolidation of individual particles, agglomerates or clusters, extraneous defects, such as porosity, insufficient bonding, and impurities are sometimes introduced leading to the degradation of ductility. In this study we propose to examine the hypothesis that deformation can be used to ameliorate the negative effects of these artifacts on the ductility of NS alloys. The approach involved cryomilling and forging to synthesize bulk NS nickel with porosity (95.5% theoretical density) and nitrogen grain boundary (GB) segregation. The results demonstrate that cold rolling resulted in an increase in tensile ductility from 2 to ~4%, with a slight decrease in yield strength from 1150 to 1050 MPa. Microstructural analyses suggest that the elimination of nano-porosity together with the physical breakdown of a continuous nitrogen layer at GBs during cold rolling is possibly responsible for the observed ductility enhancement, and in the case of the latter phenomena, a corresponding decrease in strength also.

© 2009 Elsevier B.V. All rights reserved.

### 1. Introduction

Bulk nanostructured (NS) materials can be synthesized via a variety of techniques which can generally be grouped into two broad categories: “top down” typically involving plasticity mechanisms (e.g., severe plastic deformation (SPD) [1]) and “bottom up” involving the assembly of individual units (e.g., self assembly, inert gas condensation [2] and ball milling [3]). Inspection of the scientific literature shows that bulk NS materials are synthesized via consolidation of individual particles, agglomerates or clusters using cold/hot isostatic pressing (CIP/HIP) [4], quasi-isostatic Ceracon forging [5], and spark plasma sintering (SPS) [6], to name a few. Despite encouraging results it is evident that extraneous defects, such as porosity, insufficient bonding and impurities are sometimes introduced during consolidation, and that these effectively degrade ductility.

The poor ductility of NS materials has emerged as a key obstacle that has prevented widespread application of these materials [7–9]. The low ductility of bulk, artifacts-free, NS materials, such as those prepared by SPD methods, is generally attributed to their intrinsic microstructural factors related to deformation mechanisms, such as high density of lattice imperfections and small-size grains resulting in a low strain-hardening ability. According to Considère's crite-

rium [10], a high strain-hardening rate is essential for good uniform elongation because it can help delay necking instabilities.

The presence of processing artifacts in bulk NS materials that are synthesized via consolidation of individual particles, agglomerates or clusters further degrades the intrinsically low ductility of these materials. For example, in 1997, Weertman et al. performed detailed investigations on the influence of processing porosity on the mechanical properties of nanocrystalline Cu and Pd prepared by inert gas condensation (IGC) and subsequent consolidation, and found that the pores could cause premature failure under tensile stresses sometimes even before yielding has a chance to start as well as a decrease in strength [11,12]. Moreover, impurities are more susceptible to segregation in bulk NS materials given the increased grain boundary (GB) volume in these materials [13–20]. The short diffusion distance from the grain interior to the boundary and the presence of a high density of lattice defects in a NS alloy will significantly enhance the likelihood of GB segregation. The influence of GB segregation on the mechanical behavior of NS materials depends on the type of impurity, and it will either increase GB bonding [13,14] or decrease GB bonding [15–18]; the former enhancing the strength of the material and the latter leading to decohesion and embrittlement. Impurity elements that generally improve strength include: B, C, N in the case of Ni [13], whereas harmful impurity elements include: S, P and Bi for Ni and Cu, etc. [13,15–18]. It is important to note that, regardless of whether the impurity elements result in increased strength or GB decohesion, it is reported that GB segregation generally degrades the ductility of

\* Corresponding author. Tel.: +1 530 7529568; fax: +1 530 7529554.  
E-mail address: [yhzhao@ucdavis.edu](mailto:yhzhao@ucdavis.edu) (Y.H. Zhao).

**Table 1**

Chemical compositions of the as-forged Ni sample analyzed in two commercial laboratories (Luvak Inc., Boylston, MA; Leco Corp., St. Joseph, MI). The impurities sought were C, O, N, H, Fe, Al, Mn, Cr and Ti. Both laboratories gave the comparable results.

	C (wt.%)	O (wt.%)	N (wt.%)	H (wt.%)	Fe (wt.%)	Al (wt.%)	Mn (wt.%)	Cr (wt.%)	Ti (wt.%)	Ni (wt.%)
Luvak Inc.	0.103	0.091	0.39	0.00008	0.17	0.018	0.0024	0.013	0.0024	99.2%
Leco Corp.	0.101	0.088	0.35	<0.2 ppm	–	–	–	–	–	–

Methods: Oxygen and nitrogen, inert gas fusion—ASTME 1019-03.

Carbon, combustion infrared detection—ASTME 1019-03.

Hydrogen, inert gas fusion—ASTME 1447-05.

All others, direct current plasma emission spectroscopy—ASTME 1097-03.

NS materials [19,20]. This is because GB strengthening by the impurity segregation might limit the mobility of GBs [21] by diminishing grain rotation [22–25] and dislocation nucleation at the GBs [26].

In view of the above discussion, the objective of present study was to develop a strategy for improving the poor ductility of bulk NS alloys with artifacts prepared by a “bottom up” consolidation process without incurring significant loss in strength, and to provide insight into the underlying deformation mechanisms.

## 2. Experimental

A bulk NS Ni sample with porosity and N segregated on the GBs was prepared by cryomilling and quasi-isostatic (QI) forging [27,28]. Nanocrystalline Ni powders with a grain size of approximately 10 nm were prepared by cryomilling commercially pure Ni powders (>99.7 wt.%) in liquid argon. Stainless steel balls with a diameter of 6.4 mm were used as the grinding media with a ball-to-powder mass ratio of 30:1. 0.2 wt.% stearic acid ( $\text{CH}_3(\text{CH}_2)_{16}\text{COOH}$ ) was used as a process control agent to limit particle-to-particle welding during deformation. In an inert atmosphere glove box, the 150 g cryomilled Ni powders were placed in stainless steel can and degassed under vacuum of about  $10^{-3}$  Pa first at a temperature of 450 °C for 24 h followed by a second degassing step at a temperature of 810 °C for 2.5 h. The degassed cans were then QI forged at 800 °C to form a bulk NS Ni disk (with a thickness of 20 mm and a diameter of 50 mm). Chemical composition analysis and density measurement indicate that the forged NS Ni has a purity of 99.2% and a density of 8.51 g/cm<sup>3</sup> (95.5% of Ni theoretical density). The principal impurities are N, Fe and C, which originate from the milling media [27,28], as listed in Table 1. A portion of the forged disk (with a thickness of 10 mm and a diameter of 50 mm) was rolled in thickness reduction of 20% with the rolling direction normal to the forging direction. The density of the rolled sample is 8.61 g/cm<sup>3</sup> (96.6% of Ni theoretical density).

Dog-bone shaped cylinder tensile specimens with a gauge length of 10 mm and a diameter of 3 mm were machined from the forged disks with a gauge direction perpendicular to the forging direction. The rolled plate was electro-discharge machining (EDM) into specimens with a gauge section of 2 mm × 2 mm × 10 mm. Four tensile specimens were produced for each sample to establish repeatability of results. The tensile tests were performed on an Instron 8801 universal testing machine (UTM) using Bluehill 2 software at a strain rate of  $10^{-3}$  and  $10^{-4}$  s<sup>-1</sup>. The strain was measured by using a standard non-contacting video extensometer with a 100 mm field of view lens.

Microstructures of the as-forged and rolled Ni samples were characterized using transmission electron microscopy (TEM), energy-filtering TEM (EFTEM), X-ray diffraction (XRD), scanning electron microscopy (SEM) and atomic force microscopy (AFM) measurements. TEM observation was carried out on a Philips CM12 microscope operated at 100 kV. The energy-filtered TEM images were taken by using a FEI Tecnai F20. To prepare TEM specimens, small pieces were sectioned from the forged and rolled samples, and polished into thin foils with thicknesses of about 50 μm. The thin foils were twin-jet electro-polished by a solution (75 vol.%

nitric acid +25 vol.% methanol) for several minutes at a voltage of 7 V and a temperature of 235 K. The fracture surface was imaged by a FEI-XL30 SFE SEM using a 25 kV beam. Quantitative XRD measurements were performed on a Scintag X-ray diffractometer equipped with a Cu target operating at 1.8 kW. The pores were studied using a Nanoscope<sup>®</sup> IIIa Scanning Probe Microscope operating in a tapping mode. The AFM sample was finally polished by diamond suspension with a particle size of 50 nm. The densities of the as-forged and rolled Ni samples were measured using an AG204 Mettler Toledo Balance at room temperature. Ethanol was used as auxiliary liquid to avoid bubbles on the sample surface. A thermometer was used to measure the temperature of the ethanol from which its density can be determined. The density of pure Ni reference (with a purity of 99.99%) was measured as 8.91 g/cm<sup>3</sup>.

## 3. Results

### 3.1. Mechanical properties

The representative engineering stress–strain curves of the rolled and as-forged (unrolled) samples are compared in Fig. 1. It is apparent that the forged sample has a 0.2% yield strength of 1150 MPa (marked by an open circle), a uniform elongation of 1.5% (marked by black arrow) and a tensile ductility of 2%. Rolling slightly lowers the yield strength to 1050 MPa, and ultimate tensile strength from 1240 to 1160 MPa, but evidently enhances the uniform elongation to 2.2% (pointed by black arrow) and doubles the tensile ductility to 4%. The strength and ductility errors are within 20 MPa and 0.5%, respectively. When the rolled sample was tested at a strain rate of  $10^{-4}$  s<sup>-1</sup>, the uniform elongation and ductility increased to 2.8

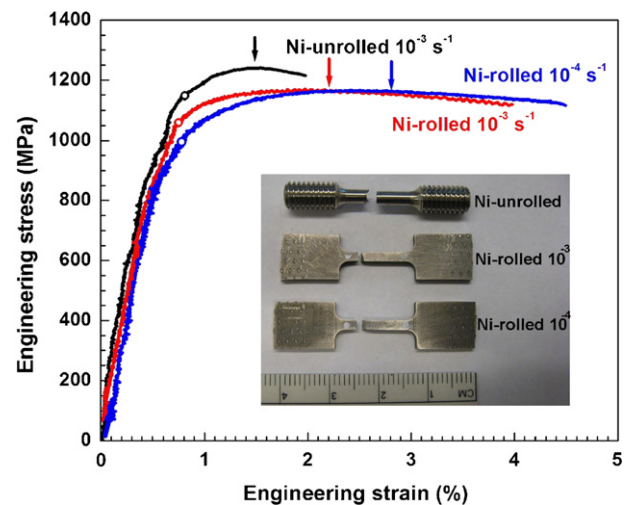


**Fig. 1.** Tensile engineering stress–strain curves of the rolled and unrolled Ni samples. The inset shows fractured tensile specimens with gauge dimensions of 10 mm × 2 mm × 2 mm for rolled Ni, and 10 mm × 3 mm for unrolled Ni. The yield strength was marked by open circle, and the ultimate tensile strengths of the samples were designated by arrows, respectively. Two strain rates ( $10^{-3}$  and  $10^{-4}$  s<sup>-1</sup>) were used for the rolled Ni sample.

**Table 2**

Comparison of yield strength  $\sigma_{0.2}$ , ultimate tensile strength  $\sigma_{UTS}$ , uniform elongation  $\epsilon_{ue}$  and elongation to failure  $\epsilon_{ef}$  of the rolled and unrolled Ni samples. The strength and ductility errors are 20 MPa and 0.5%, respectively.

Samples	Strain rate ( $s^{-1}$ )	$\sigma_{0.2}$ (MPa)	$\sigma_{UTS}$ (MPa)	$\epsilon_{ue}$ (%)	$\epsilon_{ef}$ (%)
Ni-unrolled	$10^{-3}$	1150	1240	1.5	2.0
Ni-rolled	$10^{-3}$	1050	1160	2.2	4.0
	$10^{-4}$	1000	1160	2.8	4.5

and 4.5%, respectively, as listed in Table 2. It is worth noting that recently we reported that specimen geometry and size can significantly affect the tensile stress–strain curves [29,30]. However, the different tensile ductility between the rolled and forged samples used in present work is not attributable to differences in geometries, because they have the same gauge length, and according to our analyses, the larger gauge cross-sectional area of the forged sample (4.7 mm<sup>2</sup> versus 4.0 mm<sup>2</sup> of the rolled tensile specimen) should actually improve ductility [29,30]. Moreover, the round gauge geometry of the forged sample should benefit the necking elongation and therefore the overall elongation to failure than the square one of the rolled sample. Therefore, based on the tensile results, i.e. the tensile ductility of the rolled sample is evidently larger than that of the forged sample, we conclude that the rolling process significantly enhanced the ductility of the Ni sample and slightly lowered its yield strength.

### 3.2. Microstructures

#### 3.2.1. Grain, grain boundary and dislocation

To provide insight into the underlying origin of the enhanced tensile ductility of the rolled NS Ni, we carried out TEM, EFTEM, XRD, SEM and AFM studies. Fig. 2a presents typical bright-field TEM images and the corresponding selected area diffraction (SAD) patterns (taken from an area with a diameter of 5.0  $\mu\text{m}$ ) of the forged sample. The sample contained equi-axed grains with a size range from  $\sim 50$  to 500 nm and an average grain size of about 150 nm. Annealing twin ribbons were frequently observed (as pointed by black arrows). The grains in the forged sample reveal sharp and straight equilibrium GBs. The contrast between neighboring grains is large, thereby suggesting these are boundaries with higher misorientation angles. The ring-like SAD pattern further verifies the random grain orientations of the high-angle boundaries (HAGBs). It appears that the HAGBs of the forged Ni were formed primarily during the degassing and forging process via recrystallization and grain growth [5]. Careful TEM studies revealed a few dislocations in each grain of the forged sample, indicating that the dislocation density is low. This can be further verified by the uniform contrast observed within the grains with the exception of the twin boundaries. The dislocation density, calculated from XRD peak broadening [31,32] is approximately  $2 \times 10^{13} \text{ m}^{-2}$ .

The TEM image of the rolled sample is displayed in Fig. 2b. It is evident that a high density of dislocations is observed in the grains of the rolled Ni NS sample, as evidenced by the strong contrast variation caused by the strain field around dislocations in grains, which are in a strong diffraction condition (i.e., the grains appear dark). Fig. 2c shows a TEM image with a higher magnification. One can observe a high density of tangled dislocations within the grains introduced by the rolling deformation (as indicated by white arrows in Fig. 2c). The dislocation density calculated by XRD peak broadening of the rolled sample was increased to  $5 \times 10^{14} \text{ m}^{-2}$ , further confirmed the above TEM results. Moreover, elongated grains are observed in some areas. Although it is difficult to locate straight and sharp GBs due to the presence of deformation-induced high density of defects, one can still distinguish different grain orienta-

tions by their large contrasts (Fig. 2b). This suggests that the rolling process mainly introduced a high density of dislocations and elongated some large grains but did not significantly alter the original grain orientations. SAD patterns further verified this suggestion. The SAD pattern shown in inset of Fig. 2b was taken from an area

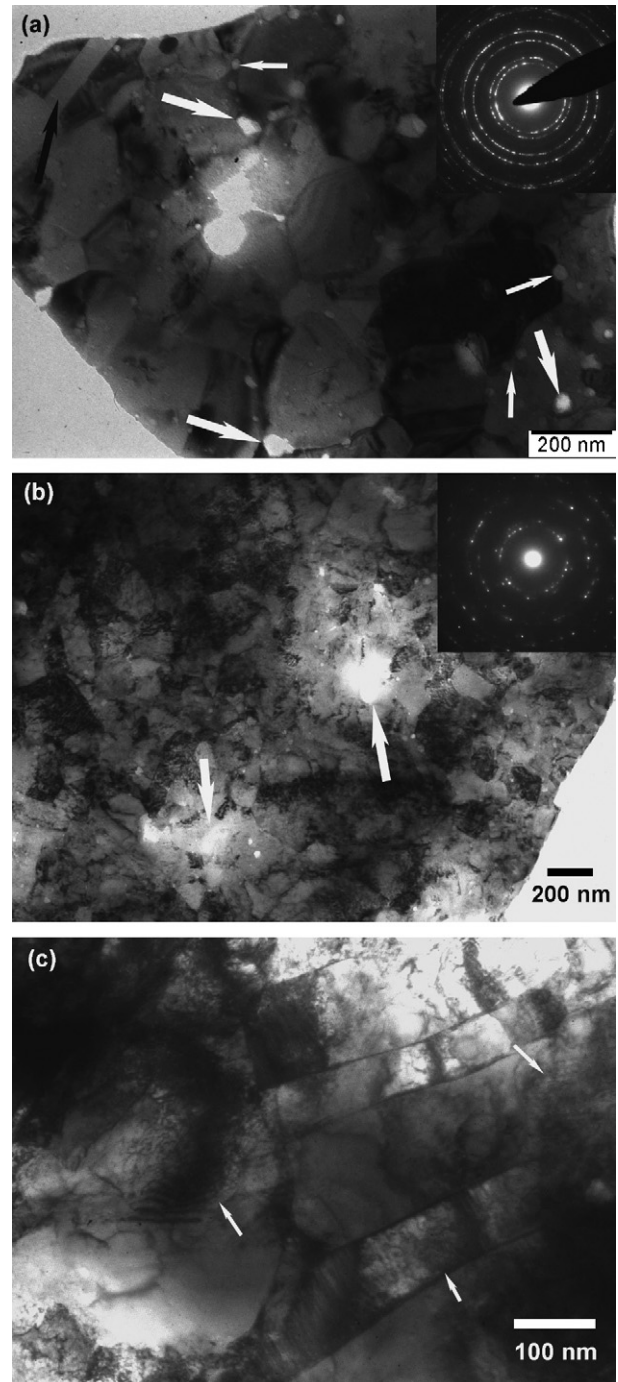


**Fig. 2.** (a) A bright-field TEM image and corresponding selected area diffraction (SAD) pattern (taken from an area with a diameter of 5.0  $\mu\text{m}$ ) of the unrolled Ni sample. Equi-axed grains with sharp and straight equilibrium boundaries and spherical bright spots (porosity, marked by white arrows) at the GBs as well as twin ribbons (marked by black arrows) are observed. (b) A bright-field TEM image and the corresponding SAD pattern (taken from an area with a diameter of 1.0  $\mu\text{m}$ ) of rolled Ni sample. Grains with high contrast variations and porosity (marked by the white arrows) are observed. (c) High-magnification TEM image for the rolled Ni sample to show elongated grains within which high-density dislocations are observed, as pointed by the white arrows.

(with diameter of about 1  $\mu\text{m}$ ) containing tens of grains. The ring-like pattern indicates that these grains are oriented with high-angle GBs.

### 3.2.2. Porosity

In view of the fact that the theoretical densities of both forged and rolled samples are not high (95.5 and 96.6%, respectively) and as discussed in Section 1, porosity has significant influence on mechanical behavior, especially the tensile ductility, we studied the morphology and distribution of the pores, as well as their evolution during the rolling process. From Fig. 2a, some spherical bright spots with sizes of several tens of nanometers were observed on the GBs, especially at the triple junctions of the GBs, as marked by the white thick arrows. Since we did not observe such bright spots in other 100% dense TEM specimens prepared by the exact same methods, we deduce that these bright spots are corresponding to pores in the forged sample. These pores might be formed via pore segregation and coalescence at the GBs during the recrystallization and grain growth processes at elevated forging temperature. Some pores are gray color because they do not pass through the electron-transparency thin film of the TEM specimens which has a thickness usually smaller than 100 nm. The average pore-to-pore distance is found to be  $\sim 1 \mu\text{m}$ , which is much larger than the grain size and suggests that not every triple junction contains a pore. Large area TEM observation also revealed a few large pores, several hundreds of nanometers in diameter. We used AFM surface morphology analyses to study these large pores, as shown in Fig. 3 for the polished as-forged Ni sample. Cavities are observed with an inter-cavity distance from several micrometer up to 10  $\mu\text{m}$ . The size of the cavities ranges from several hundreds of nanometer to several micrometers. These large cavities are corresponding to the large pores observed in TEM images formed during the forging process. Fig. 3b shows a typical cavity with a depth of 45 nm and a diameter of about 600 nm. Several grains/particles can be discerned in the cavities. The grains have a size of about 200 nm comparable with the grain size from TEM images, as shown in the depth profile in Fig. 3c.

From Fig. 2b, the amount of the nano-pores on the GBs was significantly reduced following cold rolling, as anticipated. A few large pores are still evident as marked by the white arrows, and can be attributed to the small rolling reduction in thickness (i.e., 20%). Experimental support to this suggestion is provided by the fact that the increase in theoretical density following rolling was relatively small (i.e., 96.6% theoretical density). Therefore, we conclude that cold rolling primarily eliminated the nano-pores at the GBs but did not significantly influence the few large pores present.

### 3.2.3. Impurity and GB segregation

According to chemical analysis results, the main impurities are N, C and Fe, as expected from the milling media used in our experiments. Fe can form homogeneous solid solution with Ni, whereas C and N are susceptible to GB segregation and strengthening [13]. In the present study, we limit our discussion to N since the amount of C is much lower than N and it has similar GB segregation as N. Energy-filtered TEM (EFTEM) has proven to be an efficient technique for determining elemental distribution on a nanometer scale [33]. In present work, N *K*-edge was used to EFTEM map N GB segregation. The bright GBs reveal extensive N segregation on the GBs, as indicated by arrows in Fig. 4. Moreover, some bright regions were also observed at grain interiors, suggesting possible transgranular N enrichment. Regardless of the extent of GB segregation, N was present as a solute, and hence not as Ni nitride. This could be verified by both SAD (inset in Fig. 2a) and XRD patterns (as shown in Fig. 5) where no Ni nitride signals were observed. The lattice parameter of the forged Ni sample was calculated as 0.3526 nm and is comparable to that of pure Ni [34]. This result indicates that

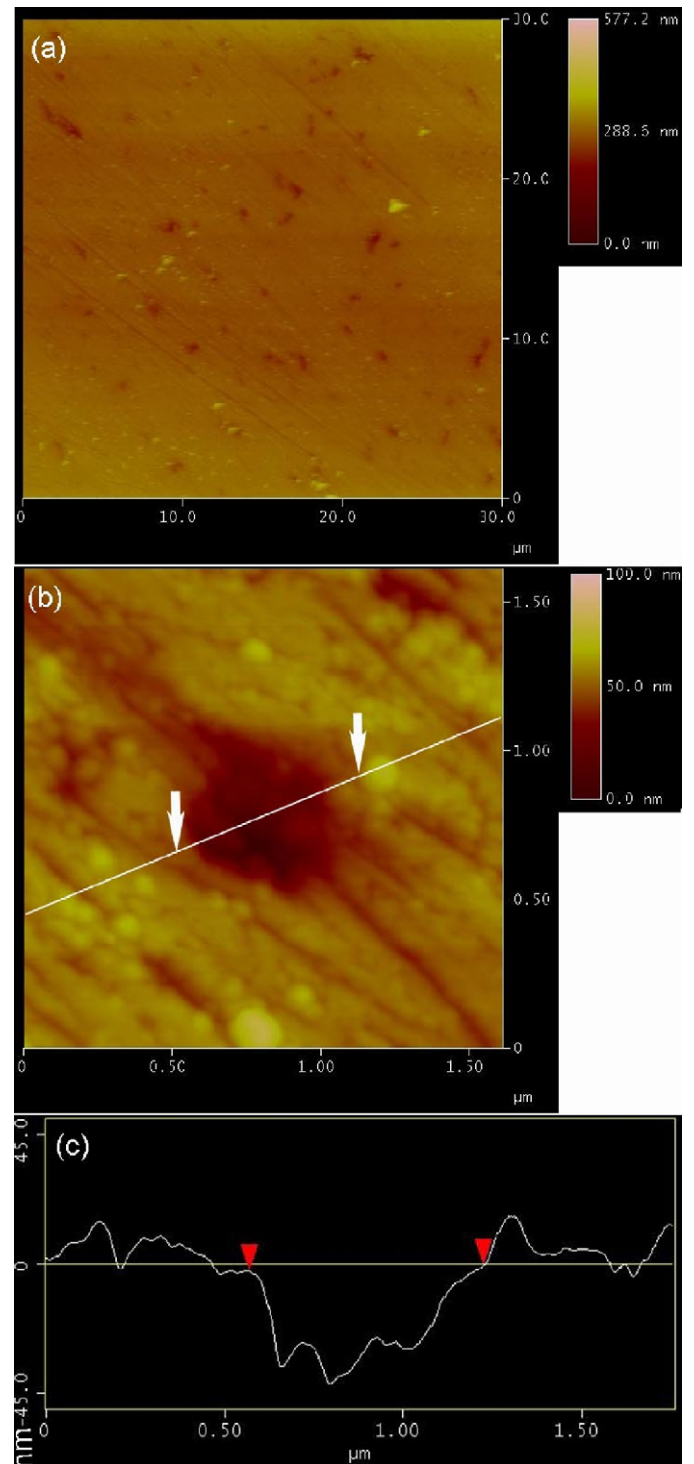


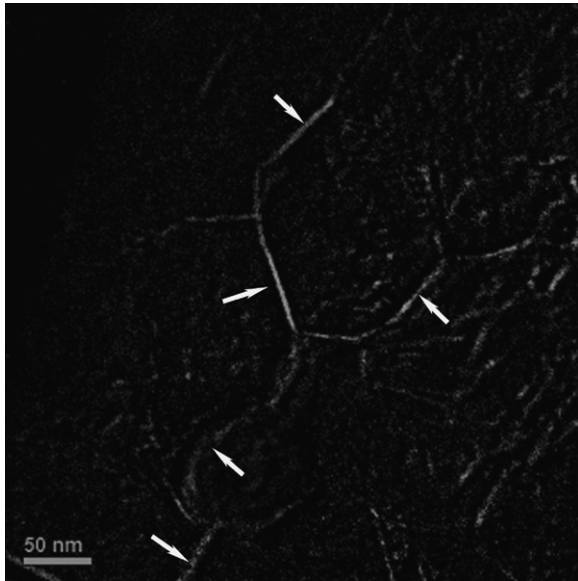
**Fig. 3.** (a) Surface topography of the polished as-forged Ni sample showing cavities with an inter-cavity distance from several hundreds of nanometer to several micrometer. (b) AFM image of a cavity where several grains/particles can be discerned. (c) Depth profile of the white line in (b) showing the cavity has a depth of about 45 nm and a diameter of about 600 nm.

most of N solute has segregated on the GBs, thereby depleting N from the Ni lattice. From Ni–N phase diagram [35], the solubility of N in Ni is negligible at room temperature which explains the occurrence of N GB segregation. The  $\text{Ni}_3\text{N}$  observed in cryomilled Ni powders [27] decomposed during degassing and forging processes at a temperature higher than 700 °C.

**Table 3**

Comparison of grain shape, dislocation density, grain boundary misorientation, density, nano-pores, N GB segregation layer of the rolled and unrolled Ni samples.

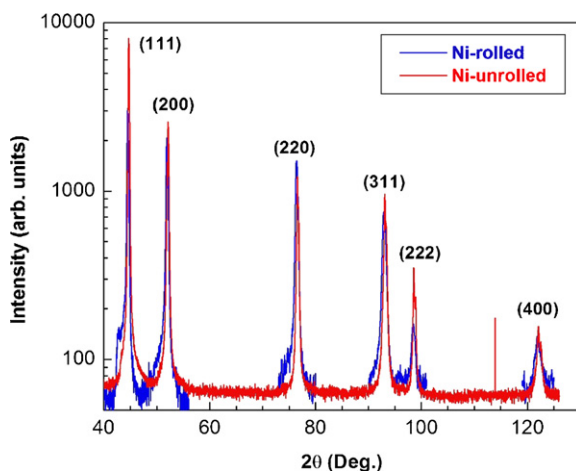
Samples	Grain shape	GB misorientation	Dislocation density ( $\times 10^{13} \text{ m}^{-2}$ )	Theoretical density (%)	Nano-pores	N GB segregation layer
Ni-unrolled	Equi-axed	High-angle GBs	2	95.5	High density	Continuous
Ni-rolled	Partially elongated	High-angle GBs	50	96.6	Low density	Distorted/fractured

**Fig. 4.** EFTEM mapping image using the N *K*-edge of the as-forged Ni sample. The GBs exhibit bright contrast, indicating the N segregation to the GBs.

It is natural to deduce that the GB segregation layer was distorted and even fractured during grain deformation. The lattice parameter of the rolled Ni sample remains constant as 0.3527 nm. Both SAD and XRD patterns of the rolled sample did not reveal any nitride signals. These results suggest that following rolling, although the GB segregation layer was fractured into discrete fragments, the N remained as a segregated solute, as opposed to be distributed homogeneously throughout the Ni lattice.

### 3.3. Fracture morphology

To provide fundamental insight into the mechanisms that govern the mechanical behavior results reported above, we further studied the failure behavior. As shown in Fig. 6a and b, the frac-

**Fig. 5.** XRD patterns of rolled and unrolled Ni samples. No Ni nitride was discerned.

ture surface of the as-forged sample is composed of small dimples with sizes ranging from 50 to 500 nm (comparable to the grain size) and large dimples with sizes of approximately 1  $\mu\text{m}$ . The small-size dimples are dominant and cover about 70% in area of the fracture surface. From the dimple morphology, we propose that both small and large dimples evolved during ductile transgranular fracture. Similar transgranular ductile fracture was reported in nanocrystalline Ni prepared by electrodeposition methods [36,37]. However, the size of the dimples (about 1  $\mu\text{m}$ ) in the electrodeposited nanocrystalline Ni is much larger than the grain size (19 nm). Three mechanisms responsible for void initiation were proposed, including existing voids at GBs and triple points, voids created by dislocation emission from GBs, and voids created by GB sliding which leaves wedges at triple junctions [37]. The spacing of these initiation sites, which is larger than the grain size, determines the dimple size. In the present study, the nano-pores and large pores certainly act as pre-existing fracture resources, which lower the tensile ductility. However, if the pores act as the unique fracture void, then the dimple size should be comparable with the pore-to-pore distance. The much smaller dimple size (50–500 nm) as compared to the average pore-to-pore distance (about 1  $\mu\text{m}$ ) suggests the presence of other void initiation sites, in addition to pores. The similarity between dimple size and grain size suggests that the N GB segregation may have influenced deformation. The presence of a non-deformable N GB segregation layer is likely to promote void initiation at the GBs during plastic deformation. In related studies, comparable dimple and grain sizes were observed in annealed nanocrystalline Ni prepared by electrodeposition [36]. This was argued to promote intergranular brittle fracture as a result of S and P impurities which segregated at GBs and weakened them [36].

As shown in Fig. 6c and d, the fracture surface of the rolled Ni sample is composed of a majority of large dimples with a size larger than 1  $\mu\text{m}$  and an area fraction of about 75% in the fracture surface area. Moreover, the size of the small dimples also increased in excess of 200 nm. A possible reason for the increased dimple size and fraction of large dimples might result from the cold rolling process which eliminated large amount of the nano-pores and fractured or distorted the N GB segregation layer. In addition, from Fig. 6d, the dimples in the rolled sample are slightly elongated due to the texture induced by cold rolling. Fig. 7 displays the side-view fracture morphology for the as-forged and rolled samples. Both samples fractured in a normal fracture mode, with a fracture surface normal to the loading axis.

## 4. Discussion

Table 3 compares the microstructural differences between the forged and the rolled samples. One can see that the subsequent rolling process elongated some large grains, increased dislocation density significantly, increased the density of the Ni by eliminating most of the nano-pores, and distorted the N GB segregation layer, but did not evidently change the GB misorientation. The increases in density and dislocation density will enhance the yield strength, while fracturing the N GB segregation layer will decrease the yield strength. Therefore, the observed slight decrease in yield strength is resulted from the overall effects of the density and dislocation density increases as well as the distortion of the N segregation layer. The

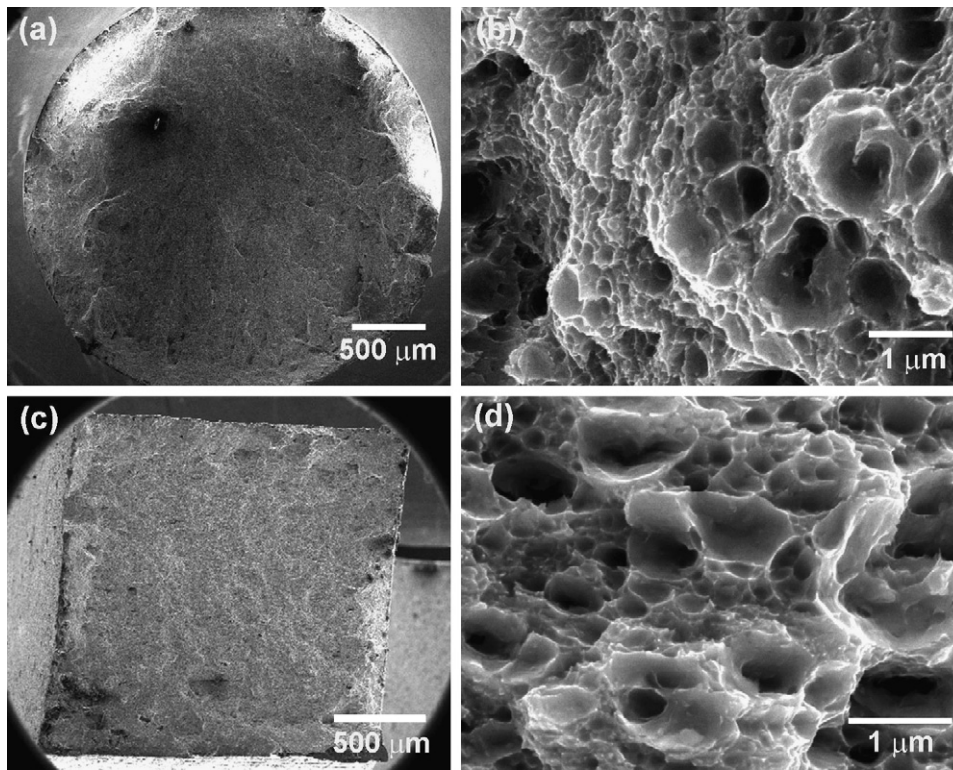


**Fig. 6.** SEM images of the fracture surfaces of the as-forged (a and b) and rolled (c and d) Ni samples. The as-forged Ni sample has similar small dimple size with its grain size, while the rolled Ni sample has much larger dimple size. The dimples in the rolled Ni sample are slightly elongated due to elongated grained structures.

decrease in yield strength also indirectly verifies the presence of distortion of the N GB segregation layer during the rolling process.

The ductility of the as-forged Ni sample is much lower than the values (about 8%) reported in literature for ultrafine grained (UFG) Ni prepared by equal-channel-angular pressing (ECAP) [38]. Both porosity and N GB segregation are thought as two main reasons for such a low ductility. The hard N segregation layer limits plastic deformation (dislocation slip) within individual grain interiors because it is difficult for dislocations to cross the hard N GB segregation layer. Moreover, the hard GB segregation layer also hinders grain rotation and GB sliding leading to void formation. This is thought to result in a fracture dimple size that is comparable to the grain size (Fig. 6b). Moreover, the high density of pre-existing nano-pores will facilitate fracture initiation, thereby decreasing ductility.

The enhanced ductility of the rolled Ni sample is thought to be caused mainly by the elimination of large amount of nano-pores, and also might be caused by the fracture and redistribution of the N GB segregation layer, which makes it possible for plastic deformation and dislocation slip to occur across GBs. This is further verified by the increase in the fracture dimple size (Fig. 6d). As discussed in the introduction part, the N GB segregation layer strengthens GB bonding but lowering GB mobility such as GB sliding or grain rotation [21]. The fracture of the N GB segregation layer enhanced the GB mobility. Although the theoretical density of the rolled sample changed only very slightly, from 95.5 to 96.6%, after rolling, large amount of the nano-pores are eliminated after cold rolling (Fig. 2b). These nano-pores have significant influence on the tensile ductility due to their high density and uniform distribution. Hence, the welding of these nano-pores will enhance the ductility. The other microstructural changes, such as dislocation density and grain morphology, might also have minor contributions to the ductility change. According to our previous work, high dislocation density is unfavorable to tensile ductility [39]. Moreover, an elongated grain morphology is not beneficial to ductility because it hinders grain rotation.

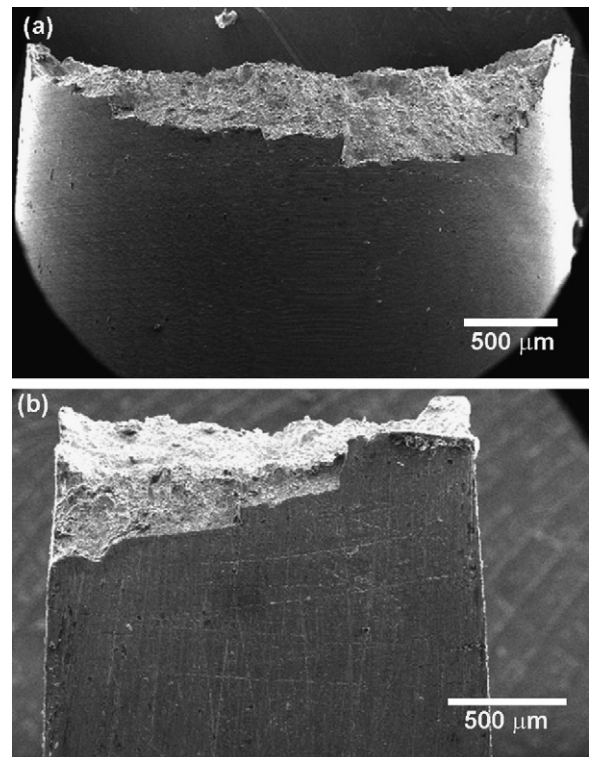


**Fig. 7.** Side-view SEM images showing fracture morphologies of the as-forged Ni (a) and rolled Ni (b) samples. Both samples failed in a normal fracture mode.

## 5. Conclusions

In summary, the present study demonstrates a simple strategy to enhance the ductility of nanostructured alloy with porosity and GB segregation *via* deformation. In details, we found:

1. Nanostructured Ni, prepared by cryomilling and forging techniques, has high-density nano-pores and N segregation on the grain boundary.
2. Rolling enhanced the ductility of the forged Ni sample from 2 to 4%, by lowering the yield strength slightly from 1150 to 1050 MPa.
3. The ductility increase of the rolled Ni sample was mainly caused by the elimination of large amount of nano-pores and probably the physical fracture of the segregation layer due to deformation.

## Acknowledgments

Y.H. Zhao and E.J. Lavernia would like to acknowledge support by the Office of Naval Research (Grant number N00014-08-1-0370) with Dr. Lawrence Kabacoff as program officer.

## References

- [1] R.Z. Valiev, R.K. Islamgaliev, I.V. Alexandrov, *Prog. Mater. Sci.* 45 (2000) 103–189.
- [2] H. Gleiter, *Prog. Mater. Sci.* 33 (1989) 223–315.
- [3] D.B. Witkin, E.J. Lavernia, *Prog. Mater. Sci.* 51 (2006) 1–60.
- [4] E.J. Lavernia, B.Q. Han, J.M. Schoenung, *Mater. Sci. Eng. A* 493 (2008) 207–214.
- [5] Y.H. Zhao, T. Topping, J.F. Bingert, A.M. Dangelewicz, Y. Li, W. Liu, Y.T. Zhu, Y.Z. Zhou, E.J. Lavernia, *Adv. Mater.* 20 (2008) 3028–3033.
- [6] U. Anselmi-Tamburini, J.N. Woolman, Z.A. Munir, *Adv. Funct. Mater.* 17 (2007) 3267–3273.
- [7] C.C. Koch, D.G. Morris, K. Lu, A. Inoue, *MRS Bull.* 24 (1999) 54–58.
- [8] C.C. Koch, *Scripta Mater.* 49 (2003) 657–662.
- [9] E. Ma, *Scripta Mater.* 49 (2003) 663–668.
- [10] G.E. Dieter, *Mechanical Metallurgy*, 3rd ed., McGraw-Hill, Boston, 1986.
- [11] P.G. Sanders, J.A. Eastman, J.R. Weertman, *Acta Mater.* 45 (1997) 4019–4025.
- [12] P.G. Sanders, C.J. Youngdahl, J.R. Weertman, *Mater. Sci. Eng. A* 234 (1997) 77–82.
- [13] L.G. wang, C.Y. Wang, *Mater. Sci. Eng. A* 234 (1997) 521–524.
- [14] L. Heatherly, E.P. George, *Acta Mater.* 49 (2001) 289–298.
- [15] R. Schweinfest, A.T. Paxton, M.W. Finnis, *Nature* 432 (2004) 1008–1011.
- [16] G. Duscher, M.F. Chisholm, U. Alber, M. Ruhle, *Nat. Mater.* 3 (2004) 621–626.
- [17] M. Yamaguchi, M. Shiga, H. Kaburaki, *Science* 307 (2005) 393–397.
- [18] A.Y. Lozovoi, A.T. Paxton, M.W. Finnis, *Phys. Rev. B* 74 (2006) 155416.
- [19] G.J. Fan, H. Choo, P.K. Liaw, *Appl. Phys. Lett.* 89 (2006) 06191.
- [20] Y.M. Wang, S. Cheng, Q.M. Wei, E. Ma, T.G. Nieh, A. Hamza, *Scripta Mater.* 51 (2004) 1023–1028.
- [21] J. Monk, B. Hyde, D. Fakas, *J. Mater. Sci.* 41 (2006) 7741.
- [22] Z.W. Shan, E.A. Stach, J.M.K. Wiezorek, J.A. Knapp, D.M. Follstaedt, S.X. Mao, *Science* 305 (2004) 654–657.
- [23] Y.B. Wang, J.C. Ho, X.Z. Liao, H.Q. Li, S.P. Ringer, Y.T. Zhu, *Appl. Phys. Lett.* 94 (2009) 011908.
- [24] J. Schiotz, K.W. Jacobsen, *Science* 301 (2003) 1357–1359.
- [25] M. Legros, D.S. Gianola, K.J. Hemker, *Acta Mater.* 56 (2008) 3380–3393.
- [26] A. Elsener, O. Politano, P.M. Derlet, H. Van Swygenhoven, *Acta Mater.* 57 (2009) 1988–2001.
- [27] J. Lee, F. Zhou, K.H. Chung, N.J. Kim, E.J. Lavernia, *Metall. Mater. Trans. A* 32 (2001) 3109–3115.
- [28] J.J. Thornton, B.Q. Han, E.J. Lavernia, *Metall. Mater. Trans. A* 38 (2007) 1343–1350.
- [29] Y.H. Zhao, Y.Z. Guo, Q. Wei, A.M. Dangelewicz, C. Xu, Y.T. Zhu, T.G. Langdon, Y.Z. Zhou, E.J. Lavernia, *Scripta Mater.* 59 (2008) 627–630.
- [30] Y.H. Zhao, Y.Z. Guo, Q. Wei, T.D. Topping, A.M. Dangelewicz, Y.T. Zhu, T.G. Langdon, *Mater. Sci. Eng. A* 525 (2009) 68–77.
- [31] L.H. Qian, S.C. Wang, Y.H. Zhao, K. Lu, *Acta Mater.* 50 (2002) 3425–3434.
- [32] Y.H. Zhao, K. Lu, K. Zhang, *Phys. Rev. B* 66 (2002) 085404.
- [33] W. Grogger, K.M. Krishnan, R.A. Ristau, T. Thomson, S.D. Harkness, R. Ranjan, *Appl. Phys. Lett.* 80 (2002) 1165–1167.
- [34] Powder Diffraction File, Joint Committee on Powder Diffraction Standards, Swarthmore, PA, 1990, No.: 04-0850.
- [35] <http://www.asminternational.org>.
- [36] C. Xiao, R.A. Mirshams, S.H. Wang, W.M. Yin, *Mater. Sci. Eng. A* 301 (2001) 35–43.
- [37] K.S. Kumar, S. Suresh, M.F. Chisholm, J.A. Horton, P. Wang, *Acta Mater.* 51 (2003) 387–405.
- [38] N. Krasilnikov, W. Lojkowski, Z. Pakielna, R. Valiev, *Mater. Sci. Eng. A* 397 (2005) 330–337.
- [39] Y.H. Zhao, J.F. Bingert, Y.T. Zhu, X.Z. Liao, R.Z. Valiev, Z. Horita, T.G. Langdon, Y.Z. Zhou, E.J. Lavernia, *Appl. Phys. Lett.* 92 (2008) 081903.